ACS central science

Research Article

http://pubs.acs.org/journal/acscii

Deciphering the Interplay among Multisite Phosphorylation, Interaction Dynamics, and Conformational Transitions in a Tripartite Protein System

Philip Lössl,[†,‡] Andrea M. Brunner,[†,‡] Fan Liu,[†,‡] Aneika C. Leney,[†,‡] Masami Yamashita,[§] Richard A. Scheltema,[†,‡] and Albert J. R. Heck*[,†,‡]

[†]Biomolecular Mass Spectrometry and Proteomics, Bijvoet Center for Biomolecular Research and Utrecht Institute for Pharmaceutical Sciences, University of Utrecht, Padualaan 8, 3584CH Utrecht, The Netherlands

[‡]Netherlands Proteomics Center, Padualaan 8, 3584CH Utrecht, The Netherlands

[§]Department of Structural Cell Biology, Max Planck Institute of Biochemistry, Am Klopferspitz 18, 82152 Martinsried, Germany

Supporting Information

ABSTRACT: Multisite phosphorylation is a common pathway to regulate protein function, activity, and interaction pattern *in vivo*, but routine biochemical analysis is often insufficient to identify the number and order of individual phosphorylation reactions and their mechanistic impact on the protein behavior. Here, we integrate complementary mass spectrometry (MS)-based approaches to characterize a multisite phosphorylation-regulated protein system comprising Polo-like kinase 1 (Plk1) and its coactivators Aurora kinase A (Aur-A) and Bora, the interplay of which is essential for mitotic entry after DNA damage-induced cell cycle arrest. Native MS and cross-linking–MS revealed that Aur-A/Bora-mediated Plk1 activation is accompanied by the formation of Aur-A/Bora and Plk1/Bora heterodimers. We found that the Aur-A/Bora interaction is independent of the Bora phosphorylation state, whereas the Plk1/Bora interaction is dependent on extensive Bora multisite phosphorylation. Bottom-up and top-down proteomics analyses showed that Bora multisite phosphorylation proceeds via a well-ordered sequence of site-specific phosphorylation reactions, whereby we could reveal the involvement of up to 16 phosphorylated Bora residues. Ion mobility spectrometry–MS demonstrated that this multisite phosphorylation primes a substantial structural rearrangement of Bora, explaining the interdependence between extensive Bora multisite phosphorylation and Plk1/Bora complex formation. These results represent a first benchmark of our multipronged MS strategy, highlighting its potential to elucidate the mechanistic and structural implications of multisite protein phosphorylation.

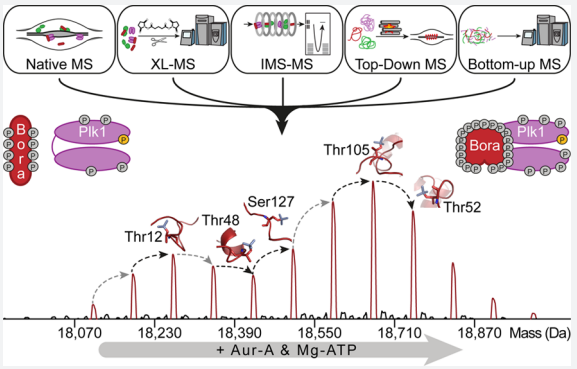

INTRODUCTION

The post-translational phosphorylation of proteins at more than one residue (multisite phosphorylation) is a long-known concept of cellular protein regulation.[1,2] Multisite phosphorylation of key regulatory proteins, such as the microtubule-associated protein tau and the tumor suppressor p53, has been related to the pathogenesis of several neurodegenerative diseases and human cancers.[3,4] Moreover, there is increasing evidence that multisite phosphorylation is a universal regulatory mechanism for the correct timing of many cell cycle related processes.[5−7] As regulatory cell cycle kinase/substrate systems are important drug targets,[8,9] a thorough molecular understanding of multisite phosphorylation in the cell cycle is crucial to reveal new druggable protein regions or highlight off-target effects of known inhibitors.[10,11] However, apart from a few fascinating exceptions,[12−15] cell cycle kinase/substrate systems have primarily been characterized with respect to their general cytophysiological function, rather than their molecular mechanism. This is mainly due to a lack of robust methods to simultaneously monitor the number, site location, and mechanistic implications of multisite protein phosphorylation. Classical biochemical methods to investigate protein phosphorylation, such as radiolabeling with [γ-^{32}P]-ATP, detection by phospho-site-specific antibodies, and phosphomimetic amino acid substitutions, are either limited in their ability to distinguish between single-site and multisite phosphorylation or require preliminary knowledge about the expected phosphorylation sites. An unbiased probing of protein phosphorylation is, in principle, facilitated by mass spectrometry (MS)-based high-throughput phosphoproteomics, but, as phosphorylation patterns are typically identified at the peptide level, information on the interdependence and sequence of individual phosphorylation reactions is mostly lost. Moreover,

Received: February 29, 2016
Published: June 10, 2016

DOI: 10.1021/acscentsci.6b00053
ACS Cent. Sci. 2016, 2, 445−455

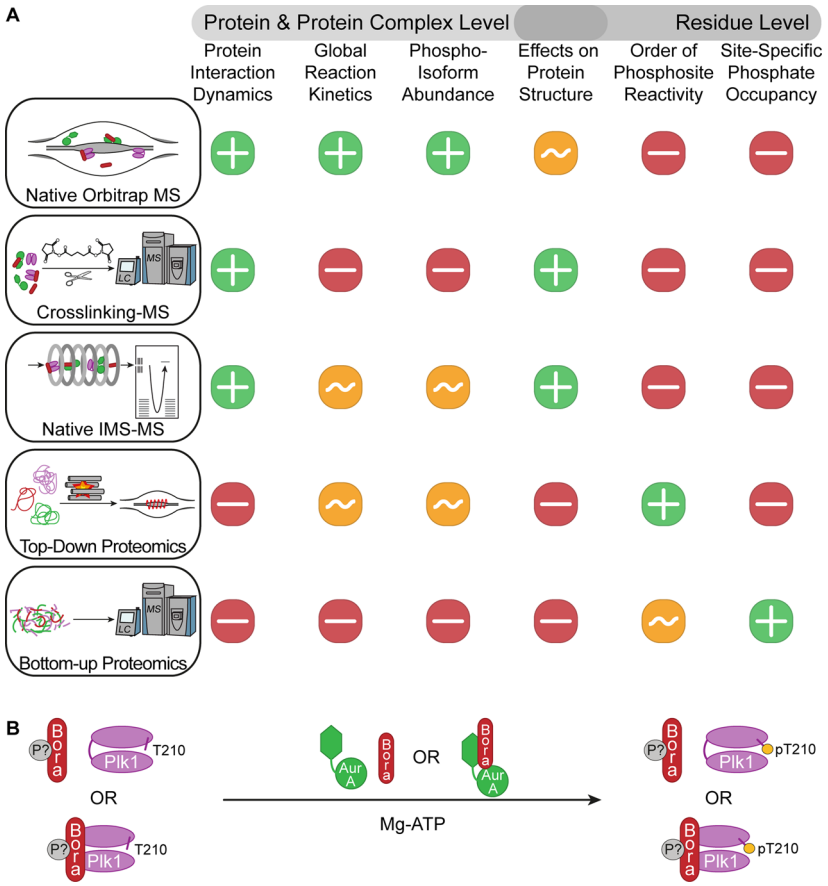

Figure 1. Analyzing multisite phosphorylation and protein complex formation by integrating mass spectrometric strategies. (A) Mechanistic aspects of multisite phosphorylation that can be addressed by complementary MS techniques. Techniques that are best suited to monitor a certain aspect are indicated by "+". Techniques that allow the detection of some but not all features related to a certain aspect are denoted by "∼". (B) Current mechanistic knowledge of the Aur-A/Bora-catalyzed Plk1 activation. Plk1 is activated through phosphorylation of Thr210, which is jointly catalyzed by Aur-A and Bora. Although Bora is known to contain binding and phosphorylation sites of Aur-A and Plk1, it is unclear whether and how protein complex formation and Bora phosphorylation affect Plk1 activation.

none of the aforementioned methods provide a direct readout for structural implications of the phosphorylation process, such as conformational changes or protein complex formation, which are often critical for the mechanistic understanding of multisite phosphorylation.[12,15−17]

Thus, analytical tools are needed to characterize multisite phosphorylation in molecular detail, specifically the reaction kinetics at protein and protein complex level, the differential reactivity of the phosphorylatable amino acids, and the occurrence of phosphorylation-induced cooperative effects on protein structures or interaction patterns. We have previously shown that a subset of these aspects, namely, phosphorylation kinetics and protein interactions, can be simultaneously probed by high-resolution MS analysis under nondenaturing conditions (native MS)[18] using an Orbitrap EMR mass analyzer.[19,20] Most importantly, high-resolution native MS enables the detection and mass separation of all differentially phosphorylated protein and protein complex species (phospho-isoforms), even if their relative mass differences are as little as 0.05%.[18] Next to native MS, there are several complementary MS-based strategies, such as cross-linking−MS, top-down proteomics, and ion mobility spectrometry (IMS)−MS, that can be used to probe additional aspects of multisite phosphorylation (Figure 1A). Cross-linking−MS reveals (phosphorylation-dependent) protein interactions and conformations in solution by covalent chemical linkage and subsequent MS-based identification of the cross-linked residues.[21,22] Top-down proteomics approaches facilitate the localization of phosphorylated residues on individual phospho-isoforms by sequencing the intact proteins in the gas phase.[23] This provides information on the sequential order of residue-specific phosphorylation reactions and, if combined with peptide-centric bottom-up proteomics, also the extent of phosphorylation on each residue.[24−26] Furthermore, IMS−MS can monitor the influence of phosphorylation on the conformational dynamics of proteins and protein complexes,[27,28] as it gives information on the shape and size of proteins based on their drift time through a gas-filled mobility cell.[29] Together, these methods provide different information about the phosphorylation reaction but require the same initial sample preparation steps, starting from an *in vitro* kinase reaction under physiological conditions. Therefore, they can be readily combined to elucidate multisite protein phosphorylation processes in a reasonable time frame and with minimal sample consumption (Figure 1A).

In our previous proof-of-concept studies on multisite phosphorylation, we used either top-down proteomics[24] or a combination of native MS and bottom-up proteomics[18] to probe the binary Aur-A kinase domain/Bora and Plk1/Bora systems. We hypothesized that integrating these strategies with the above-mentioned complementary MS methods enables the mechanistic investigation of systems with more complex phosphorylation and interaction patterns. Therefore, we set

DOI: 10.1021/acscentsci.6b00053
ACS Cent. Sci. 2016, 2, 445−455

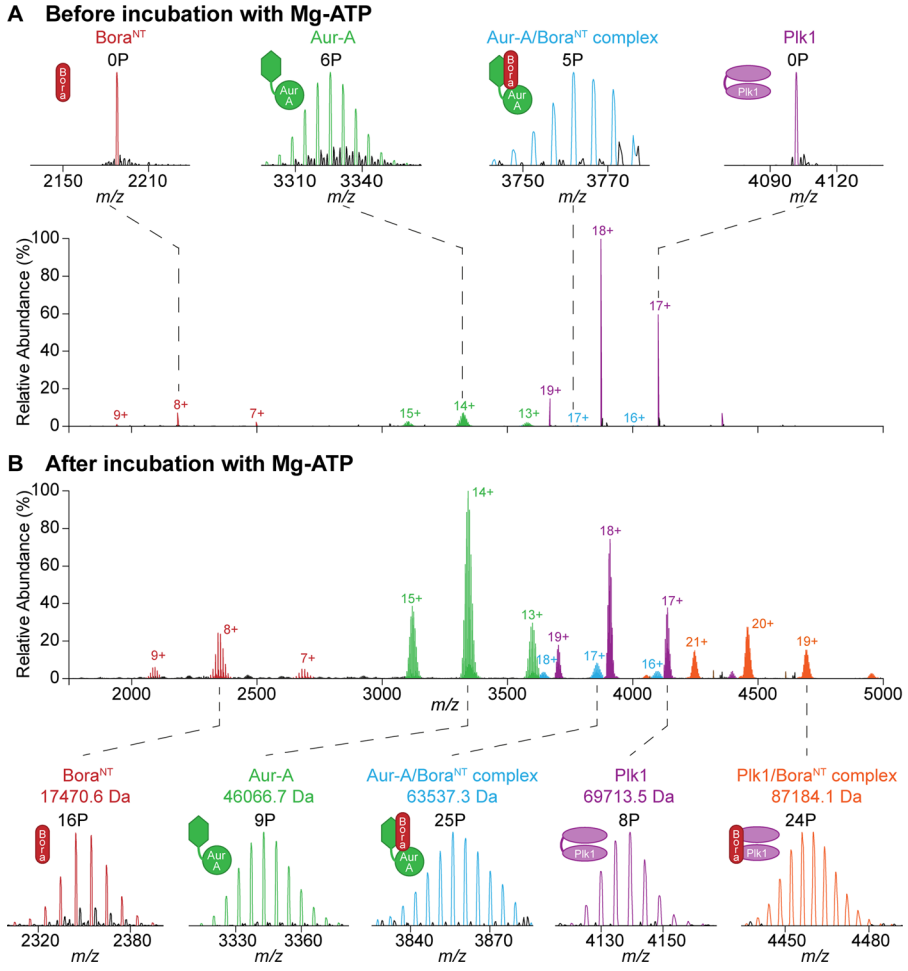

Figure 2. Monitoring the Aur-A/Bora^{NT}/Plk1 system with native MS. Shown are mass spectra of an equimolar mixture (5 μM) of Aur-A, Bora^{NT}, and Plk1 before (A) and after (B) 5 h incubation with Mg-ATP. Peaks are labeled with their respective charge state and colored according to the protein species they represent. The detected protein and protein complex species, the expected molecular weight of their unphosphorylated isoform, and the number of phosphorylations (P) on their most abundant phospho-isoform are indicated in the insets of A and B.

out to characterize the phosphorylation-induced activation of Polo-like kinase 1 (Plk1) by full-length Aurora kinase A (Aur-A) and its protein cofactor Bora, a complex and biologically relevant three protein system in which the role of multisite phosphorylation remains to be deciphered. Plk1 activation is essential for cells to enter mitosis after recovery from a DNA damage-induced cell cycle arrest, as shown by a wide range of *in vivo* studies.[30−33] While the cytophysiological implications of Plk1 activation have been described in detail, its molecular mechanism is still poorly understood. To date, it is only known that Plk1 is activated through the Aur-A-catalyzed phosphorylation of Thr210 and that this process is augmented by the Aur-A activator Bora (Figure 1B).[32,33] Bora is a largely disordered protein that becomes multiply phosphorylated *in vivo* by several kinases.[34−36] Its N-terminal domain is a stable interaction partner and a phosphorylation substrate of Aur-A,[37] suggesting that Aur-A activation involves the Bora N-terminus. Interestingly, the Bora N-terminus can also be bound and phosphorylated by Plk1.[31] Neither the specific sites nor the functions of these N-terminal Bora phosphorylations have yet been characterized. Additionally, Plk1 can phosphorylate Bora at its C-terminal residues Ser497 and Ser501, resulting in Bora degradation.[31,38] This degradation process will not be studied since it commences after the initial Aur-A/Bora-mediated Plk1 activation. Here, we aim to characterize the complex interplay of Plk1, Aur-A, and the Bora N-terminus (residues 1−150, from here on termed Bora^{NT}) in mechanistic detail, specifically focusing on the implications of the Bora^{NT} phosphorylation status, its phosphorylatable sites, and the sequential interactions among the three proteins.

Using native MS and cross-linking−MS, we demonstrate that Aur-A/Bora^{NT} complex formation is independent of the Bora^{NT} phosphorylation state. In contrast, substantial Plk1/Bora^{NT} complex formation depends on the extensive Plk1- and Aur-A-catalyzed multisite phosphorylation of Bora^{NT}, with more than 75% of its Ser and Thr residues being phosphorylated. With top-down and quantitative bottom-up proteomics approaches, this Bora^{NT} multisite phosphorylation could be fully characterized at the amino acid residue level. Pushing the limits of top-down proteomics, we localize up to 16 Bora^{NT} phosphorylation sites and define the order by which Plk1 and Aur-A process these substrate sites. By means of IMS−MS, we observe that these phosphorylation events induce a significant conformational change of Bora^{NT}, providing a rationale for the correlation between Bora^{NT} multisite phosphorylation and enhanced Plk1/Bora^{NT} complex formation. Together, the complementary mass spectrometric data give detailed molecular insights into the Aur-A/Bora/Plk1 reaction mechanism, emphasizing the potential of our integrated MS approach to

DOI: 10.1021/acscentsci.6b00053
ACS Cent. Sci. 2016, 2, 445−455

comprehensively describe the mechanistic principles and structural consequences of multisite phosphorylation.

RESULTS

Time-Resolved Native MS Analysis Elucidates the Interplay between Multisite Phosphorylation and Stable Interactions in the Tripartite Aur-A/Bora^{NT}/Plk1 System. Our MS-based strategy is centered on high-resolution native Orbitrap MS, as it provides an accurate readout for all phosphorylation events at the protein and protein complex level. Previously, this has enabled us to qualitatively prove stable complex formation between the Aur-A kinase domain and Bora^{NT}, while simultaneously following the Aur-A-catalyzed Bora^{NT} phosphorylation.[18] To probe the interplay of Aur-A, Bora^{NT}, and Plk1, we employ high-resolution native MS in such a way that allows us to monitor not only protein phosphorylation states but also the relative abundances of emerging noncovalent protein complexes (see Supporting Information). Representative native mass spectra obtained for a mixture of Aur-A, Bora^{NT}, and Plk1 before and after incubation with Mg-ATP (see Figure S1 for sequences and domain architecture of the three proteins) are shown in Figure 2. The native mass spectra show ion signals of all individual proteins and the binary noncovalent Aur-A/Bora^{NT} and Plk1/Bora^{NT} heterodimers. Before incubation with Mg-ATP, the mass spectrum exhibits single peaks for the Bora^{NT} and Plk1 charge states, illustrating that they are completely unphosphorylated (Figure 2A, insets). In contrast, the Aur-A charge states are split into a fine structure of peaks, representing different phospho-isoforms. This is due to the autophosphorylation activity of Aur-A during recombinant production in *Escherichia coli*.[39] After incubation with Mg-ATP, different phospho-isoforms are detected for all present species, demonstrating that multisite phosphorylation is a universal characteristic of the Aur-A/Bora^{NT}/Plk1 interplay (Figure 2B, insets). These protein isoforms differ by only 80 Da (the mass of a phosphate group), yet they are fully baseline resolved in the native Orbitrap mass spectra. This superior mass resolution, which outperforms any gel- or chromatography-based protein separation method, enables precise relative phospho-isoform quantitation and the determination of intensity-weighted average phosphorylation states to derive phosphorylation progress curves.[18]

Comparing the native mass spectra before and after incubation with Mg-ATP highlights three main characteristics of the Aur-A/Bora^{NT}/Plk1 interplay. First, Plk1 is multiply phosphorylated by Aur-A, demonstrating the existence of additional substrate sites next to the well-known activation site Thr210. Second, the noncovalent Aur-A/Bora^{NT} complex is formed with and without addition of Mg-ATP, whereas the noncovalent Plk1/Bora^{NT} complex is only detected in the presence of Mg-ATP, when all proteins have become phosphorylated. Third, Bora^{NT}, which contains 28 Ser and Thr residues, displays extensive multisite phosphorylation, with its most abundant phospho-isoforms carrying 16−17 phosphorylations. As a consequence, also the Aur-A/Bora^{NT} and Plk1/Bora^{NT} heterodimers display extensive multisite phosphorylation.

Since full-length Bora is known to enhance the catalytic activity of Aur-A toward Plk1,[30,32,33] we initially examined whether Bora^{NT} shows the same effect during *in vitro* Plk1 activation. To this end, the Plk1 phosphorylation state was analyzed after 1 h incubation with Bora^{NT} and/or Aur-A (Figure S2A). Unphosphorylated Plk1 remained the most abundant species after incubation with either Bora^{NT} or Aur-A alone. Adding Aur-A and Bora^{NT} in combination, however, renders 2−3× phosphorylated Plk1. This confirms that Bora^{NT}, just as full-length Bora, enhances the Aur-A-mediated Plk1 phosphorylation.

The positive effect of Bora^{NT} during Plk1 activation could be due to Aur-A/Bora^{NT} complex formation, since the Aur-A/Bora^{NT} heterodimer seems to be continuously present in the Aur-A/Bora^{NT}/Plk1 system (Figure 2). To probe this hypothesis, we followed the Aur-A/Bora^{NT}/Plk1 reaction using native MS. The corresponding phosphorylation progress curves are shown in Figure S2B. It becomes apparent that already at the third time point, i.e., after 10 min, all species contain more than one phosphorylation. At this point, conventional (e.g., radiolabeling-based) *in vitro* kinase assays would report phosphate incorporation in all species, complicating the further monitoring of the reaction. Since our high-resolution native MS approach distinguishes all individual phospho-isoforms (Figure 2), we are able to confidently follow the reaction beyond single-site phosphorylation and probe Aur-A/Bora^{NT}/Plk1 multisite phosphorylation, which takes more than 5 h to complete. This rather long time frame indicates that the numerous phosphorylatable sites within the Aur-A/Bora^{NT}/Plk1 system span a wide range of reactivities.

In parallel, we also monitored the Aur-A/Bora^{NT}/Plk1 reaction with respect to the relative Aur-A/Bora^{NT} complex abundance in the presence and absence of Mg-ATP. Under both conditions, the Aur-A/Bora^{NT} complex abundance remained constant (Figure 3A, upper graph), although adding Mg-ATP caused progressive phosphorylation of both the Aur-A/Bora^{NT} complex and its constituent monomers (Figures S2B and 3A, lower graph). Aur-A/Bora^{NT} complex formation in the presence of Plk1, therefore, does not depend on the Bora^{NT} phosphorylation state. When the Aur-A/Bora^{NT} complex formation was probed in the absence of Plk1, however, we found that Aur-A binds less efficiently to unphosphorylated Bora^{NT} than to Bora^{NT} that had been prephosphorylated prior to the binding experiment (Figure 3B). This phosphorylation dependence of the Aur-A/Bora^{NT} interaction appears to be somehow mitigated by Plk1. Interestingly, the Aur-A/Bora^{NT} complex abundance remains the same when Plk1 is replaced by the Plk1-K82R mutant (Figure S2C), which is catalytically inactive and does not stably associate with Bora^{NT} (see Figure S3). Thus, Aur-A/Bora^{NT} heterodimerization seems to be influenced by the mere presence of Plk1, rather than its kinase activity or its stable binding to Bora^{NT}. Possibly, this effect could be caused by short-lived interactions between Plk1 and the Aur-A/Bora^{NT} complex. In summary, we observe that the Aur-A/Bora^{NT} complex forms stably throughout the Aur-A/Bora^{NT}/Plk1 reaction and that this process is directly affected by the presence of Plk1. This suggests a direct involvement of the Aur-A/Bora^{NT} heterodimer in the Plk1 activation process.

In contrast to the continuously present Aur-A/Bora^{NT} heterodimer, the Plk1/Bora^{NT} complex only became significantly abundant after Aur-A, Bora^{NT}, Plk1, and Mg-ATP had reacted for 40−60 min (Figure 4A). At different reaction times, we determined the phosphorylation state of the Plk1/Bora^{NT} complex in comparison with the sum of phosphorylations found on the concomitantly detected Plk1 and Bora^{NT} monomers (Figure 4A, solid vs dashed gray line). These phosphorylation curves overlapped during the first 20 min of the reaction when Plk1/Bora^{NT} complex abundance was still

DOI: 10.1021/acscentsci.6b00053
ACS Cent. Sci. 2016, 2, 445−455

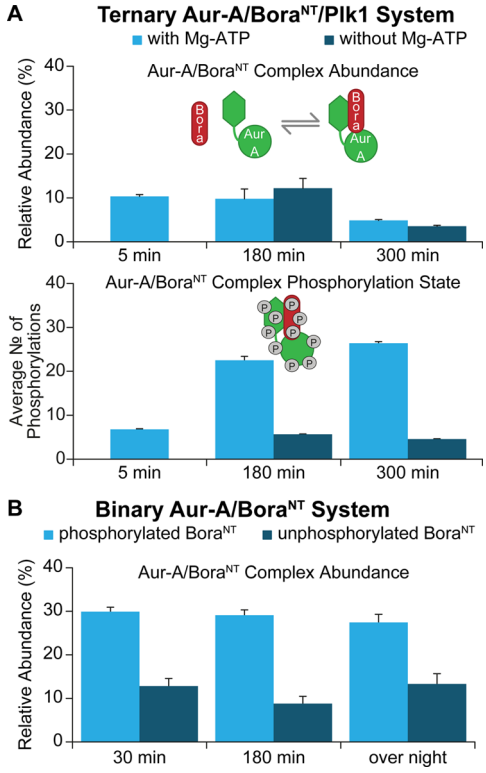

Figure 3. Aur-A/Bora^{NT} complex formation and phosphorylation. (A) Abundance (upper plot) and phosphorylation state (lower plot) of the Aur-A/Bora^{NT} complex in the presence of Plk1. Shown are three time points of the reaction monitored in the presence of Mg-ATP. Additionally, two control reactions without Mg-ATP were allowed to proceed for 180 and 300 min, respectively. (B) Complex formation between Aur-A and unphosphorylated or prephosphorylated Bora^{NT} in the absence of Plk1 (no Mg-ATP added during the binding experiment). Bora^{NT} was prephosphorylated by overnight incubation with catalytic amounts of Aur-A, yielding 3−4× phosphorylated Bora^{NT} isoforms. The corresponding phosphorylation sites have been described previously.[18] The relative complex abundances were calculated as the intensity ratio of Bora^{NT}-bound Aur-A to total Aur-A, considering all present phospho-isoforms. Error bars represent standard deviations from duplicates.

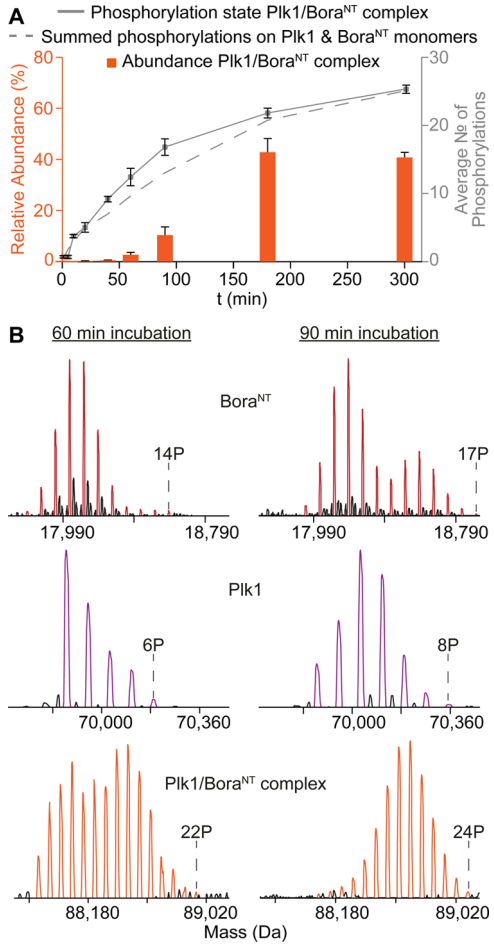

Figure 4. Plk1/Bora^{NT} complex formation and phosphorylation. (A) Evolution of phosphorylation state and abundance of the Plk1/Bora^{NT} complex over time, as derived from the native MS experiments in the presence of Aur-A and Mg-ATP. The number of phosphorylations was calculated as a weighted average based on the phospho-isoform intensities in the native mass spectra. The relative complex abundance was calculated as the intensity ratio of Bora^{NT}-bound Plk1 to total Plk1, considering all present phospho-isoforms. Error bars represent standard deviations from duplicates. (B) Zero charge state mass spectra of Bora^{NT}, Plk1, and the Plk1/Bora^{NT} complex after 60 and 90 min of incubation, demonstrating the earlier appearance of the bimodal phospho-isoform distribution in the Plk1/Bora^{NT} complex as compared to Bora^{NT}. The highest phosphorylation state detected for each species (P) is indicated.

marginal. This indicates that, at this stage, Plk1 and Bora^{NT} associate irrespective of their phosphorylation states. However, the phosphorylation curves started to deviate as soon as the rapid increase in Plk1/Bora^{NT} complex abundance was observed (Figure 4A). At this point of the reaction, the Plk1/Bora^{NT} complex exhibited substantially higher phosphorylation states than its constituent monomers. As such, Plk1/Bora^{NT} complex formation may be promoted by the extensive multisite phosphorylation of its constituents, from here on termed "hyperphosphorylation". In the mass spectra, this hyperphosphorylation coincided with a bimodal mass distribution of the Plk1/Bora^{NT} complex phospho-isoforms (Figure 4B, left panel). Interestingly, a bimodal phospho-isoform distribution was also observed for the Bora^{NT} monomer, transitioning to hyperphosphorylated Bora^{NT} when >10 phosphorylations are present, but not for the Plk1 monomer (Figure 4B). Therefore, the bimodal phospho-isoform distribution and apparent hyperphosphorylation of the Plk1/Bora^{NT} complex is likely caused by the binding of Plk1 to hyperphosphorylated Bora^{NT}. Notably, the bimodal phospho-isoform distribution was initially most clearly seen in the Plk1/Bora^{NT} complex, whereas higher Bora^{NT} phosphorylation states were severely depleted (Figure 4B, left panel). A clear bimodal phospho-isoform distribution for unbound Bora^{NT} was only detected after the Plk1/Bora^{NT} complex had become fully hyperphosphorylated (Figure 4B, right panel). These results suggest that Plk1 interacts preferentially with hyperphosphorylated Bora^{NT}, resulting in more efficient Plk1/Bora^{NT} complex formation (see also Figure 5A for the results of complementary SDS−PAGE-based assays, which will be discussed later on).

As both Bora^{NT} hyperphosphorylation and Plk1/Bora^{NT} heterodimerization were observed in native MS, we set out to investigate whether these phenomena are interdependent. Plk1 and Bora^{NT} contain distinctive kinase-specific substrate sites that become readily modified.[24,32,33] Therefore, we first speculated that preliminary phosphorylation of these sites on Plk1 or Bora^{NT} might be sufficient to facilitate Plk1/Bora^{NT}

DOI: 10.1021/acscentsci.6b00053
ACS Cent. Sci. 2016, 2, 445−455

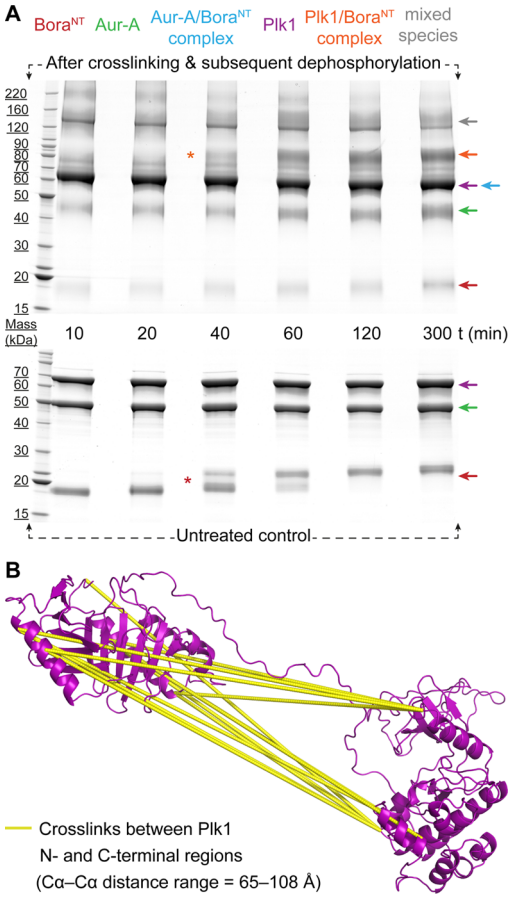

Figure 5. Aur-A/Bora^{NT}/Plk1 interactions studied by chemical cross-linking. (A) The Aur-A/Bora^{NT}/Plk1 reaction time course monitored by SDS−PAGE. Samples were either chemically cross-linked and subsequently dephosphorylated (upper gel) or left untreated (lower gel). The occurrence of the Plk1/Bora^{NT} complex and Bora^{NT} hyperphosphorylation are respectively indicated by orange and red asterisks. The detected species are designated by arrows. The gray arrow denotes a group of bands at 120−160 kDa, which represent, according to MS analysis, a mixture of different species including complexes of dimeric Plk1 (~139 kDa), Plk1/Aur-A 1:1 (~116 kDa), Plk1/Bora^{NT} 2:1 (~157 kDa), and possibly Aur-A/Bora^{NT}/Plk1 1:1:1 (~134 kDa), all of which likely arise from low-affinity or less stable interactions (see also Figure S4). (B) Cross-links connecting the N- and C-terminal Plk1 regions mapped onto a Plk1 homology model (Figure S7A). The cross-links were identified after incubating Aur-A, Bora^{NT}, and Plk1 for 5 h with and without Mg-ATP.

complex formation without Bora^{NT} hyperphosphorylation. To test this hypothesis, we prephosphorylated Plk1 or Bora^{NT} (see Figure S3A), subsequently added the respective interaction partner at a 1:1 molar ratio, and monitored Plk1/Bora^{NT} complex formation for 1 h. Under all tested prephosphorylation conditions, less Plk1/Bora^{NT} complex was formed compared with our initial experiment, where we incubated stoichiometric amounts of Aur-A, Bora^{NT}, and Plk1 without pretreatment (Figure S3A). Thus, prephosphorylation of the most reactive substrate sites within Bora^{NT} and Plk1 is not sufficient for efficient Plk1/Bora^{NT} heterodimerization, evidencing that a stable Plk1/Bora^{NT} interaction requires higher phosphorylation states, likely achieved by the subsequent phosphorylation of less reactive sites.

Next, we asked whether the Plk1/Bora^{NT} interaction necessitates the kinase activity of both Plk1 and Aur-A. Replacing wild-type Plk1 by the kinase-inactive mutant Plk1-K82R prevented both Bora^{NT} hyperphosphorylation and stable Plk1/Bora^{NT} complex formation during 5 h of incubation (Figure S3B). The same effect occurred when only wild-type Plk1 but no Aur-A was present in the reaction mix. Adding Aur-A after 5 h, however, led to an immediate increase in phosphorylation levels and to formation of the Plk1/Bora^{NT} complex, which was again accompanied by preferred association of Plk1 with hyperphosphorylated Bora^{NT} (Figure S3C).

In summary, our native MS results demonstrate that Plk1/Bora^{NT} heterodimerization depends on the activity of both Aur-A and Plk1 and is closely related to Bora^{NT} hyperphosphorylation. By contrast, Aur-A/Bora^{NT} heterodimerization is independent of kinase activities and observed throughout the Aur-A/Bora^{NT}/Plk1 reaction.

Cross-Linking−MS Confirms the Aur-A/Bora^{NT}/Plk1 Interaction Pattern and Reveals the Intramolecular Organization of Plk1. Complementary to the native MS experiments, we followed the Aur-A/Bora^{NT}/Plk1 reaction in the presence of Mg-ATP with cross-linking−MS to obtain information on inter- and intramolecular protein interactions. These interactions were captured by amine-reactive chemical cross-linking using the popular bis(sulfosuccinimidyl)suberate (BS3) cross-linker. The cross-linked species were subsequently dephosphorylated to prevent phosphorylation-dependent electrophoretic mobility shifts and separated by SDS−PAGE (Figure 5A, upper gel). In line with the native MS data, gel bands with molecular weights corresponding to the binary Aur-A/Bora^{NT} and Plk1/Bora^{NT} complexes were readily detected (Figure 5A, blue and orange arrows). Additionally, we observed a band that corresponds to a mixture of different species (Figure 5A gray arrow), possibly including transiently formed protein assemblies (Figure S4). This supports our hypothesis that some species, notably the Aur-A/Bora^{NT} complex and Plk1 (see Figure 3), may affect each other through short-lived interactions.

As the Aur-A/Bora^{NT} complex is more abundant when Bora^{NT} is phosphorylated in the absence of Plk1 (Figure 3B), we used these conditions to probe the Aur-A/Bora^{NT} binding interface. We identified 16 intermolecular Aur-A/Bora^{NT} cross-links (Figure S5, Table S1). While 12 of these cross-links involve the highly mobile, and thus structurally less informative, protein N-termini, we also identified four lysine−lysine cross-links connecting less flexible protein regions, which render more stringent distance information. These cross-links point to an interaction between Bora^{NT} and C-terminal regions of Aur-A (Figure S5), confirming the previous observation that Bora^{NT} forms a stable complex with the C-terminal Aur-A kinase domain.[18]

While the continuously formed Aur-A/Bora^{NT} complex represents a typical target for cross-linking−MS, this technique can also be used to study nonpermanently formed interactions,[21] such as the Plk1/Bora^{NT} complex. Strikingly, the time-dependent Plk1/Bora^{NT} complex formation can be precisely monitored with chemical cross-linking, as evidenced by the emergence of an 88 kDa band on SDS−PAGE after 40 min reaction time (Figure 5A, orange asterisk in upper gel). The identity of the Plk1/Bora^{NT} complex was proven by bottom-up proteomics analysis of the respective gel band, revealing six intermolecular Plk1/Bora^{NT} cross-links (Figure S6A, Table S1).

In parallel to the cross-linking experiment, we left half of the reaction mix untreated (no cross-linking and dephosphoryla-

DOI: 10.1021/acscentsci.6b00053
ACS Cent. Sci. 2016, 2, 445−455

tion), allowing us to analyze the progressive phosphorylation of the three single proteins simultaneously to their interaction pattern (Figure 5A, lower gel). Remarkably, the phosphorylated Bora^{NT} monomer splits into two differently migrating gel bands (Figure 5A, red asterisk in lower gel) around the time when Plk1/Bora^{NT} complex formation was first observed (Figure 5A, orange asterisk in upper gel). This effect is likely related to the Bora^{NT} phosphorylation state, since phosphorylation frequently causes considerable mobility shifts on SDS−PAGE.[40] The detection of two clearly separated bands implies the coexistence of differentially phosphorylated Bora^{NT} isoforms at the same time point. Bimodal phospho-isoform distributions were also seen by native MS, first for the Plk1/Bora^{NT} complex and later for unbound Bora^{NT} (Figure 4B). These results support the notion that the bimodality is observed as a result of Bora^{NT} hyperphosphorylation, resulting in enhanced Plk1/Bora^{NT} complex formation.

MS analysis of the Plk1/Bora^{NT} heterodimer gel band (Figure 5A, orange asterisk in upper gel) also revealed nine intramolecular cross-links within Plk1. These cross-links shed light on the conformation of Plk1 during its activation, providing structural information that is complementary to the protein interaction data shown above. Several intramolecular cross-links connect N- and C-terminal Plk1 regions, suggesting a globular conformation for phosphorylated, Bora^{NT}-bound Plk1 (Figure S6A). This is particularly interesting since previous investigations of the Plk1 conformation led to controversial results. On the one hand, it was proposed that phosphorylation-induced activation and Bora binding trigger a conformational opening of Plk1, separating its N- and C-terminal domains.[33,41] On the other hand, a recent study suggested that the N- and C-terminal domains remain associated upon Plk1 phosphorylation/activation.[42] To further inquire into this controversy, we probed the structures of phosphorylated Bora^{NT}-bound Plk1, phosphorylated monomeric Plk1, and unphosphorylated monomeric Plk1 in a separate cross-linking−MS experiment. In all these cases, cross-links between the N- and C-terminal Plk1 regions were always observed (Figure S6B). We mapped these cross-links on a Plk1 homology model adopting an opened conformation (Figure S7A). In this model, all cross-links between the Plk1 N- and C-terminus fall beyond the maximum Cα−Cα distance of 38 Å that can be bridged by the BS3 cross-linker (Figure 5B).[43] In contrast, all cross-links within the structurally well-characterized Plk1 kinase domain exhibit Cα−Cα distances below 25 Å, demonstrating the structural validity of our cross-linking−MS approach (Figure S7B). Consequently, the cross-linking−MS data strongly suggest that Plk1 does not undergo a conformational opening but retains a closed conformation throughout the Aur-A/Bora^{NT}/Plk1 reaction.

Bottom-Up and Top-Down Proteomics Reveal the Sequence of Phosphorylation Reactions Leading to Plk1 Activation and Bora^{NT} Hyperphosphorylation. According to our analysis of the Aur-A/Bora^{NT}/Plk1 reaction at protein and protein complex level, two phosphorylated species are of particular interest. On the one hand, Plk1 becomes multiply phosphorylated by Aur-A, raising the question whether the known substrate site Plk1-Thr210[30,32,33] is the primary Aur-A target in our assays. On the other hand, we have established that Bora^{NT} hyperphosphorylation is critical for Plk1/Bora^{NT} complex formation, encouraging a detailed investigation of the site-specific phosphorylation reactions accompanying Bora^{NT} hyperphosphorylation.

First, we applied bottom-up proteomics to locate Plk1 residues that become phosphorylated in the presence of Aur-A and Bora^{NT}. To this end, we proteolyzed Plk1 with trypsin and determined the extent of residue-specific phosphorylation at peptide level using relative quantitation (see Supporting Information). Quantitative bottom-up analysis revealed that Thr210 on Plk1 is the most reactive Aur-A phosphorylation site and becomes fully modified within 10 min (Figure 6A). The

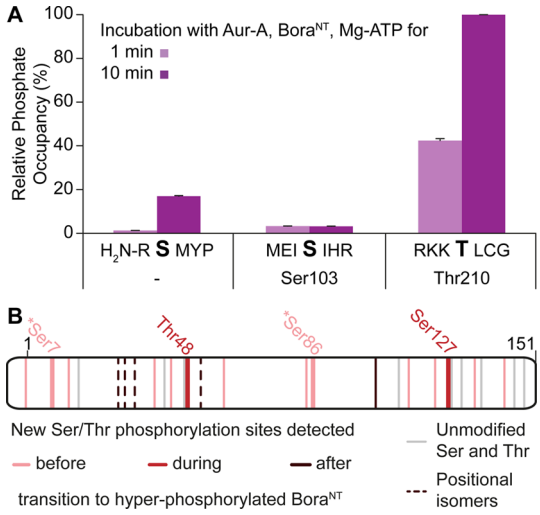

Figure 6. Mapping of phosphorylation sites by peptide-centric bottom-up (A) and protein-centric top-down (B) proteomics approaches. All residues are numbered according to Figure S1. (A) Plk1 phosphorylation sites mapped by bottom-up proteomics analysis of Plk1 peptides after tryptic digestion. The site-specific phosphate occupancy was determined by relative quantitation. Error bars represent standard deviations from duplicates. (B) Bora^{NT} phosphorylation sites mapped by top-down analysis of 7−16× phosphorylated intact Bora^{NT} (see also Table S3). Bora^{NT} is shown as a sequence bar with all Ser and Thr residues being represented as vertical lines. Depending on the Bora^{NT} phospho-isoform in which these residues were first found to be phosphorylated, they are grouped in three categories: detected before hyperphosphorylation (i.e., in the 7−10× phosphorylated isoforms), detected during hyperphosphorylation (i.e., in the 11−13× phosphorylated isoforms), and detected after hyperphosphorylation (i.e., in the 14−16× phosphorylated isoforms). Ser7 and Ser86 are labeled with an asterisk because they become partially modified before Bora^{NT} hyperphosphorylation but their phosphate occupancy substantially increases during the hyperphosphorylation process, as shown by quantitative bottom-up analysis (Table S2).

secondary and tertiary phosphorylation sites are clearly less reactive (16% and 3% phosphorylation occupancy after 10 min). This shows that Aur-A phosphorylates its primary *in vivo* substrate Plk1-Thr210 with high specificity, substantiating the functional validity of our *in vitro* assays.

Second, quantitative bottom-up proteomics was applied to analyze the gel bands corresponding to differentially phosphorylated Bora^{NT} (Figure 5A, lower gel). The clear separation of intermediately phosphorylated and hyperphosphorylated Bora^{NT} on SDS−PAGE allowed us to locate three residues—Ser7, Thr48, and Ser86—that were substantially more phosphorylated in hyperphosphorylated Bora^{NT} (Table S2). This is most apparent for Thr48, which is entirely unphosphorylated in intermediately phosphorylated Bora^{NT} but shows 83% phosphorylation occupancy upon Bora^{NT} hyperphosphorylation. An exhaustive description of the Bora^{NT}

DOI: 10.1021/acscentsci.6b00053
ACS Cent. Sci. 2016, 2, 445−455

hyperphosphorylation process using bottom-up proteomics was prevented by incomplete sequence coverage and by the fact that Bora^{NT} analysis at the peptide level generally precludes the assignment of phosphorylation sites to specific Bora^{NT} phosphorylation states. Such an assignment, however, can be obtained by top-down proteomics, where intact proteins are analyzed by MS, enabling the specific sequencing of individual phospho-isoforms.[24] This readily reveals the phosphorylation sites corresponding to each Bora^{NT} phospho-isoform, providing information on the sequence of phosphorylation events and potential crosstalk between phosphorylation sites. Moreover, Bora^{NT} species with the same number of phosphorylations but different phosphorylation sites, so-called positional isomers, can be deciphered, as we have previously shown.[24] The presence of these positional isomers, however, also presents a particular challenge for top-down proteomics.[44] In general, top-down analyses are highly demanding because the gas-phase fragmentation of intact proteins produces numerous large and highly charged fragment ions, complicating the interpretation of the mass spectra.[23,24] So far, top-down proteomics has been successfully applied to proteins with up to five post-translationally modified residues.[45] To overcome these boundaries, we performed individual top-down analyses of the 7−16× phosphorylated Bora^{NT} isoforms and used an in-house developed workflow (Brunner et al., manuscript in preparation, see Supporting Information for a brief description) to establish their respective modified sites (Table S3, Figure S8). Reassuringly, 7× phosphorylated Bora^{NT} contained all phosphorylation sites that are most reactive according to our bottom-up proteomics data and our previous top-down proteomics analysis of singly and doubly phosphorylated Bora^{NT}.[24] Noteworthy, the number of phosphorylations on intact Bora^{NT} (detected in the precursor ion mass spectrum before fragmentation) was usually lower than the number of (partially) phosphorylated residues (detected in the fragment ion mass spectra after fragmentation). This shows that most of the phospho-isoforms indeed comprise several positional isomers with different combinations of phosphorylation sites. Consequently, some of the sequential steps toward the next highest phospho-isoform merely presented a "filling up" of partially modified sites. Still, from our data it became apparent that Bora^{NT} hyperphosphorylation follows a defined succession of site-specific modifications, since the vast majority of phosphorylations had a unique starting point and we never found more than two novel phosphorylations occurring in the same phospho-isoform (Table S3).

A summary of all phosphorylation events detected with top-down proteomics at different stages of Bora^{NT} hyperphosphorylation is provided in Figure 6B. Consistent with the bottom-up proteomics results, Thr48 becomes phosphorylated during the transition to hyperphosphorylated Bora^{NT}, which proceeds when >10 phosphorylations are added (see Figure 4B). Additionally, this transition is accompanied by the modification of Ser127 (Figure 6B). Together with the increased phosphorylation of Ser7 and Ser86 upon Bora^{NT} hyperphosphorylation, shown by quantitative bottom-up proteomics (Table S2), we thus localized four phosphorylation reactions that are indicative for the transition to hyperphosphorylated Bora^{NT}.

IMS−MS Reveals a Phosphorylation-Induced Conformational Change of Bora^{NT}. The observation of bimodal Bora^{NT} phospho-isoform distributions with native MS and SDS−PAGE (Figures 4B and 5A) indicates a rapid increase in phosphorylation levels, which is likely attributable to four site-specific phosphorylation events, as extracted from the top-down and bottom-up proteomics data. Based on this finding, we hypothesized that the rapidly elevated Bora^{NT} phosphorylation state is related to a conformational change of Bora^{NT} that exposes previously protected Ser/Thr residues, allowing them to become phosphorylated by Aur-A/Plk1. To test this hypothesis, we probed the phosphorylation-dependence of the Bora^{NT} conformation by performing IMS−MS experiments on the equimolar Aur-A/Bora^{NT}/Plk1 reaction mix. As the mass spectra of the 8× charged Bora^{NT} monomer illustrate, we were able to distinguish the different Bora^{NT} phosphorylation states (Figure 7, top panel), although the mass resolving power

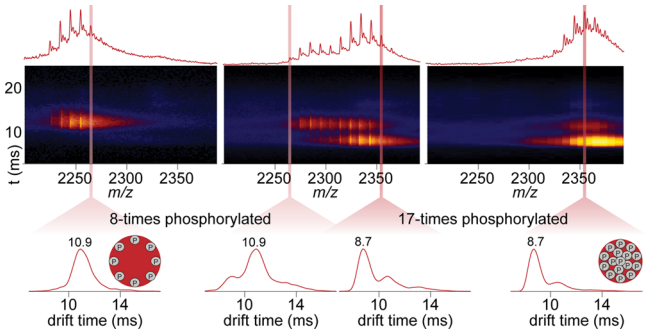

Figure 7. Structural analysis of Bora^{NT} by IMS−MS. Mass spectra (top panel) and m/z vs drift time plots (middle panel) of the 8+ charge state of Bora^{NT} before (left), during (middle), and after (right) hyperphosphorylation. The bottom panel includes the drift time distributions of 8× and 17× phosphorylated Bora^{NT}, which were extracted from the spectra displayed above (indicated by shaded funnels).

of the used IMS−MS instrument (Synapt G1) is substantially lower than that of the native MS instrument (Orbitrap EMR). Moreover, we could reproduce the bimodal distribution of Bora^{NT} phosphorylation states, previously observed with native Orbitrap MS.

Strikingly, this bimodal phospho-isoform distribution concurred with a distinct bimodal distribution of drift times (Figure 7). Higher phosphorylated forms exhibited shorter drift times, implying a distinct and sudden structural compaction during hyperphosphorylation (Figure 7, middle plots). After passing the bimodal state, the Bora^{NT} phospho-isoforms traveled almost uniformly with the shorter drift time (Figure 7, right plots), suggesting that later phosphorylation events do not have an added effect on the Bora^{NT} conformation.

Similar results were obtained after hyperphosphorylating Bora^{NT} with catalytic amounts of Aur-A and Plk1, underpinning that the observed conformational change of Bora^{NT} only depends on its extensive phosphorylation and not on stable complex formation with Plk1 or Aur-A (Figure S9). Consequently, both Bora^{NT} hyperphosphorylation and its related conformational change appear to be critical prerequisites for the Plk1/Bora^{NT} heterodimerization.

DISCUSSION

Benefits of an Integrated MS-Based Approach for the Investigation of Multisite Phosphorylation. Here, we used a multifaceted mass spectrometric approach to investigate the multisite phosphorylation-regulated tripartite system Aur-A/Bora^{NT}/Plk1. First, native MS was used to decipher the protein

DOI: 10.1021/acscentsci.6b00053
ACS Cent. Sci. 2016, 2, 445−455

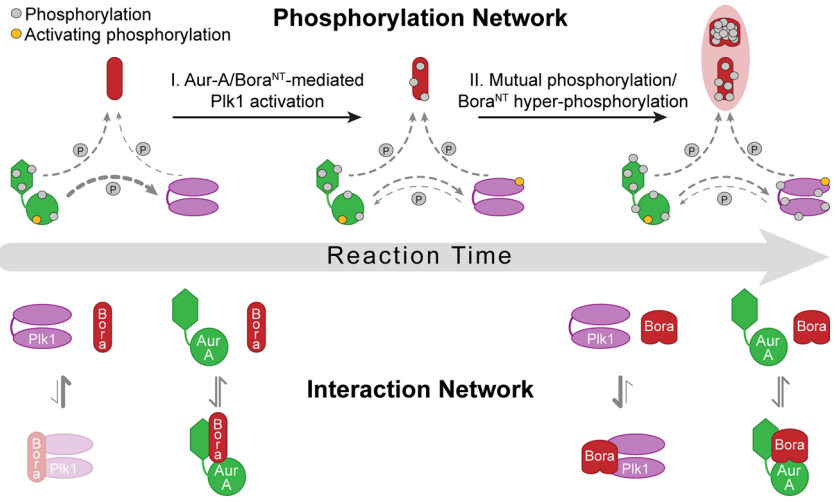

Figure 8. Interaction and phosphorylation dynamics within the tripartite Aur-A/Bora^{NT}/Plk1 system. The Aur-A/Bora^{NT}/Plk1 interplay is characterized by the initial efficient Aur-A/Bora^{NT}-catalyzed Plk1 activation, followed by the mutual enzymatic phosphorylation of all components, which eventually leads to hyperphosphorylation and conformational compaction of Bora^{NT} (indicated by red shading). This last step shifts the Plk1/Bora^{NT} binding equilibrium toward the Plk1/Bora^{NT} complex, allowing substantial complex formation. In contrast, the Aur-A/Bora^{NT} complex is continuously present, raising the possibility that this complex acts as the Plk1 activator.

interactions that occur during multisite phosphorylation, as it can preserve such noncovalent interactions in the gas phase. Thus, high-resolution native MS is ideally suited for the simultaneous probing of protein complex abundances and phosphorylation states (Figures 3 and 4). Complementary, cross-linking–MS was applied to monitor the protein interaction patterns, capturing these interactions covalently in solution. Cross-linking–MS, as we have shown, provides information on stable and transient protein complexes, binding interfaces, and protein conformations (Figures 5 and S4–S6). Next, advanced top-down proteomics experiments were conducted to unambiguously localize multiple phosphorylation sites and reveal the sequential order of these phosphorylation reactions, while bottom-up proteomics analyses were performed to add quantitative information on the extent of site-specific phosphate incorporation (Figure 6). Finally, IMS–MS was employed to monitor protein conformations in the context of their phosphorylation and binding state (Figure 7). Our results demonstrate that integrated MS approaches combine the strength of each individual, yet diverse, MS technique. This enables, for the first time, the concurrent probing of overall phosphorylation kinetics, residue-specific reactivities, protein interaction dynamics, and structural transitions. As a result, we obtained unique insights into the mutual dependence of these aspects throughout the intricate Aur-A/Bora^{NT}/Plk1 interplay.

Mechanistic Insights into the Phosphorylation and Interaction Dynamics of Aur-A, Bora^{NT}, and Plk1. It has been established that the phosphorylation-induced activation of Plk1 by Aur-A functionally depends on the presence of Bora,[30,32,33] probably involving the Bora N-terminus.[31,37] However, the molecular mechanism of this process, especially the role of multisite phosphorylation and reversible association, was yet not well understood. Our analysis revealed that this process is characterized by two critical steps, illustrating the interdependence between multisite phosphorylation and protein interaction dynamics in different varieties (Figure 8).

Initially, Aur-A and Bora^{NT} jointly catalyze the phosphorylation-induced Plk1 activation, as shown by native MS and bottom-up proteomics (Figures S2A and 6A). This mutual activity and the continuous native MS-based detection of a stable Aur-A/Bora^{NT} heterodimer, which is directly influenced by Plk1 (Figure 3), collectively suggest that the Aur-A/Bora^{NT} complex serves as the actual Plk1 activating entity, in agreement with what has been hypothesized in a recent *in vivo* study.[30] Conceivably, Plk1 activation could be triggered by an allosteric effect of Bora^{NT}, making Aur-A's active site more accessible for Plk1-Thr210. Previous hypotheses that the activation process is accompanied by a major conformational opening of Plk1[33,41] are contested by our cross-linking–MS data, which suggest a constantly closed Plk1 conformation (Figures 5B and S6). In agreement with a recent study,[42] Plk1 activation is more likely to be facilitated by relatively subtle conformational changes, which are not easily detectable with chemical cross-linking.

Subsequently, the three constituent proteins engage in mutual phosphorylations, proceeding toward Bora^{NT} hyperphosphorylation. This, in turn, enables stable Plk1/Bora^{NT} complex formation, which is evidenced by native MS and chemical cross-linking (Figures 4 and 5A). That Bora^{NT} hyperphosphorylation coincides with substantial Plk1/Bora^{NT} complex formation is likely related to a hyperphosphorylation-induced conformational switch of Bora^{NT} as indicated by its bimodal phospho-isoform distribution (Figure 4B) and its phosphorylation-induced structural compaction seen with IMS–MS (Figure 7). Moreover, IMS–MS suggests the coexistence of extended and compact Bora^{NT} conformers over several phosphorylation states. The progression between these phosphorylation states, as we have demonstrated with bottom-up and top-down proteomics, is characterized by sequential site-specific phosphorylation reactions. Specifically, we observe the (increased) phosphorylation of Ser7, Thr48, Ser86, and Ser127 (Figure 6B), which probably become exposed during the structural rearrangement of Bora^{NT}. Collectively, this supports the premise that the conformational switch of Bora^{NT}, and hence Plk1/Bora^{NT} complex formation, is induced by the sum of several Aur-A and Plk1-catalyzed phosphorylations, rather than by the modification of a single site. We can thus show that Plk1/Bora^{NT} complex formation is a consequence of Plk1 activation and not its prerequisite, as proposed earlier.[33,41]

DOI: 10.1021/acscentsci.6b00053
ACS Cent. Sci. 2016, 2, 445–455

In summary, the first step of the Aur-A/Bora^{NT}/Plk1 reaction is characterized by a stable protein interaction (Aur-A/Bora^{NT}) that appears to directly affect the protein phosphorylation dynamics (of Plk1). Conversely, the second reaction step is defined by a succession of phosphorylation reactions (Bora^{NT} hyperphosphorylation) that immediately influences protein conformations (Bora^{NT}) and stable interactions (Plk1/Bora^{NT} complex formation). The molecular mechanism of the Aur-A/Bora^{NT}/Plk1 reaction is, thus, best described as an interplay of dynamically changing phosphorylation and interaction networks (Figure 8).

These results effectively complement the existing *in vivo* data and highlight promising targets for future research. Such investigations should focus on the comprehensive elucidation of *in vivo* Bora phosphorylation states and their physiological role, whereby the here presented data provide guidelines on which sites to target. More generally, this work benchmarks what may be achieved by MS-based structural biology, in studying not only kinase−substrate relationships but any protein−protein and protein−nucleic acid system that interacts via reversible association and transfer of post-translational modifications.

■ ASSOCIATED CONTENT

Supporting Information

The Supporting Information is available free of charge on the ACS Publications website at DOI: 10.1021/acscentsci.6b00053.

Experimental procedures, Figures S1−S9, and Tables S2 and S3 (PDF)

Overview of all identified crosslinked peptides (Table S1) (XLSX)

■ AUTHOR INFORMATION

Corresponding Author

*E-mail: a.j.r.heck@uu.nl.

Notes

The authors declare no competing financial interest.

■ ACKNOWLEDGMENTS

The authors are indebted to Elena Conti (Max Planck Institute of Biochemistry) for providing the facilities for protein expression/purification. This work was supported by the ManiFold project (Grant Agreement No. 317371), embedded in the European Union seventh Framework Programme, and the Roadmap Initiative Proteins@Work (Project No. 184.032.201), funded by The Netherlands Organisation for Scientific Research (NWO). Additionally we acknowledge support from the MSMed program, funded by the European Union's Horizon 2020 Framework Programme (Grant Agreement No. 686547).

■ REFERENCES

(1) Cohen, P. The regulation of protein function by multisite phosphorylation–a 25 year update. *Trends Biochem. Sci.* **2000**, *25*, 596−601.

(2) Holmberg, C. I.; Tran, S. E. F.; Eriksson, J. E.; Sistonen, L. Multisite phosphorylation provides sophisticated regulation of transcription factors. *Trends Biochem. Sci.* **2002**, *27*, 619−627.

(3) Bode, A. M.; Dong, Z. Post-translational modification of p53 in tumorigenesis. *Nat. Rev. Cancer* **2004**, *4*, 793−805.

(4) Medina, M.; Avila, J. Further understanding of tau phosphorylation: implications for therapy. *Expert Rev. Neurother.* **2015**, *15*, 115−122.

(5) Deshaies, R. J.; Ferrell, J. E. Multisite Phosphorylation and the Countdown to S Phase. *Cell* **2001**, *107*, 819−822.

(6) Kõivomägi, M.; Ord, M.; Iofik, A.; Valk, E.; Venta, R.; Faustova, I.; Kivi, R.; Balog, E. R. M.; Rubin, S. M.; Loog, M. Multisite phosphorylation networks as signal processors for Cdk1. *Nat. Struct. Mol. Biol.* **2013**, *20*, 1415−1424.

(7) Verdugo, A.; Vinod, P. K.; Tyson, J. J.; Novak, B. Molecular mechanisms creating bistable switches at cell cycle transitions. *Open Biol.* **2013**, *3*, 120179.

(8) Lapenna, S.; Giordano, A. Cell cycle kinases as therapeutic targets for cancer. *Nat. Rev. Drug Discovery* **2009**, *8*, 547−566.

(9) Reindl, W.; Yuan, J.; Krämer, A.; Strebhardt, K.; Berg, T. Inhibition of polo-like kinase 1 by blocking polo-box domain-dependent protein-protein interactions. *Chem. Biol.* **2008**, *15*, 459−466.

(10) Shagisultanova, E.; Dunbrack, R. L.; Golemis, E. A. Issues in interpreting the in vivo activity of Aurora-A. *Expert Opin. Ther. Targets* **2015**, *19*, 187−200.

(11) Whittaker, S. R.; Walton, M. I.; Garrett, M. D.; Workman, P. The Cyclin-dependent kinase inhibitor CYC202 (R-roscovitine) inhibits retinoblastoma protein phosphorylation, causes loss of Cyclin D1, and activates the mitogen-activated protein kinase pathway. *Cancer Res.* **2004**, *64*, 262−272.

(12) Nash, P.; Tang, X.; Orlicky, S.; Chen, Q.; Gertler, F. B.; Mendenhall, M. D.; Sicheri, F.; Pawson, T.; Tyers, M. Multisite phosphorylation of a CDK inhibitor sets a threshold for the onset of DNA replication. *Nature* **2001**, *414*, 514−521.

(13) Kõivomägi, M.; Valk, E.; Venta, R.; Iofik, A.; Lepiku, M.; Balog, E. R. M.; Rubin, S. M.; Morgan, D. O.; Loog, M. Cascades of multisite phosphorylation control Sic1 destruction at the onset of S phase. *Nature* **2011**, *480*, 128−131.

(14) Kim, S. Y.; Song, E. J.; Lee, K.-J.; Ferrell, J. E. Multisite M-phase phosphorylation of Xenopus Wee1A. *Mol. Cell. Biol.* **2005**, *25*, 10580−10590.

(15) Tak, Y.-S.; Tanaka, Y.; Endo, S.; Kamimura, Y.; Araki, H. A CDK-catalysed regulatory phosphorylation for formation of the DNA replication complex Sld2-Dpb11. *EMBO J.* **2006**, *25*, 1987−1996.

(16) Bibow, S.; Ozenne, V.; Biernat, J.; Blackledge, M.; Mandelkow, E.; Zweckstetter, M. Structural impact of proline-directed pseudophosphorylation at AT8, AT100, and PHF1 epitopes on 441-residue tau. *J. Am. Chem. Soc.* **2011**, *133*, 15842−15845.

(17) Okamura, H.; Aramburu, J.; García-Rodríguez, C.; Viola, J. P.; Raghavan, A.; Tahiliani, M.; Zhang, X.; Qin, J.; Hogan, P. G.; Rao, A. Concerted dephosphorylation of the transcription factor NFAT1 induces a conformational switch that regulates transcriptional activity. *Mol. Cell* **2000**, *6*, 539−550.

(18) van de Waterbeemd, M. J.; Lössl, P.; Gautier, V.; Marino, F.; Yamashita, M.; Conti, E.; Scholten, A.; Heck, A. J. Simultaneous assessment of kinetic, site-specific, and structural aspects of enzymatic protein phosphorylation. *Angew. Chem., Int. Ed.* **2014**, *53*, 9660−9664.

(19) Rose, R. J.; Damoc, E.; Denisov, E.; Makarov, A.; Heck, A. J. High-sensitivity Orbitrap mass analysis of intact macromolecular assemblies. *Nat. Methods* **2012**, *9*, 1084−1086.

(20) Snijder, J.; van de Waterbeemd, M.; Damoc, E.; Denisov, E.; Grinfeld, D.; Bennett, A.; Agbandje-McKenna, M.; Makarov, A.; Heck, A. J. Defining the stoichiometry and cargo load of viral and bacterial nanoparticles by Orbitrap mass spectrometry. *J. Am. Chem. Soc.* **2014**, *136*, 7295−7299.

(21) Sinz, A. The advancement of chemical cross-linking and mass spectrometry for structural proteomics: from single proteins to protein interaction networks. *Expert Rev. Proteomics* **2014**, *11*, 733−743.

(22) Schmidt, C.; Zhou, M.; Marriott, H.; Morgner, N.; Politis, A.; Robinson, C. V. Comparative cross-linking and mass spectrometry of an intact F-type ATPase suggest a role for phosphorylation. *Nat. Commun.* **2013**, *4*, 1985.

(23) Compton, P. D.; Zamdborg, L.; Thomas, P. M.; Kelleher, N. L. On the scalability and requirements of whole protein mass spectrometry. *Anal. Chem.* **2011**, *83*, 6868−6874.

DOI: 10.1021/acscentsci.6b00053
ACS Cent. Sci. 2016, 2, 445−455

(24) Brunner, A. M.; Lössl, P.; Liu, F.; Huguet, R.; Mullen, C.; Yamashita, M.; Zabrouskov, V.; Makarov, A.; Altelaar, A. F.; Heck, A. J. Benchmarking multiple fragmentation methods on an orbitrap fusion for top-down phospho-proteoform characterization. *Anal. Chem.* **2015**, *87*, 4152−4158.
(25) Pan, J.; Zhang, S.; Borchers, C. H. Protein species-specific characterization of conformational change induced by multisite phosphorylation. *J. Proteomics* **2016**, *134*, 138−143.
(26) Yu, D.; Peng, Y.; Ayaz-Guner, S.; Gregorich, Z. R.; Ge, Y. Comprehensive Characterization of AMP-Activated Protein Kinase Catalytic Domain by Top-Down Mass Spectrometry. *J. Am. Soc. Mass Spectrom.* **2016**, *27*, 220−232.
(27) Lanucara, F.; Holman, S. W.; Gray, C. J.; Eyers, C. E. The power of ion mobility-mass spectrometry for structural characterization and the study of conformational dynamics. *Nat. Chem.* **2014**, *6*, 281−294.
(28) Wojnowska, M.; Yan, J.; Sivalingam, G. N.; Cryar, A.; Gor, J.; Thalassinos, K.; Djordjevic, S. Autophosphorylation activity of a soluble hexameric histidine kinase correlates with the shift in protein conformational equilibrium. *Chem. Biol.* **2013**, *20*, 1411−1420.
(29) Uetrecht, C.; Rose, R. J.; van Duijn, E.; Lorenzen, K.; Heck, A. J. Ion mobility mass spectrometry of proteins and protein assemblies. *Chem. Soc. Rev.* **2010**, *39*, 1633−1655.
(30) Bruinsma, W.; Macurek, L.; Freire, R.; Lindqvist, A.; Medema, R. H. Bora and Aurora-A continue to activate Plk1 in mitosis. *J. Cell Sci.* **2014**, *127*, 801−811.
(31) Chan, E. H. Y.; Santamaria, A.; Silljé, H. H. W.; Nigg, E. A. Plk1 regulates mitotic Aurora A function through βTrCP-dependent degradation of hBora. *Chromosoma* **2008**, *117*, 457−469.
(32) Macůrek, L.; Lindqvist, A.; Lim, D.; Lampson, M. A.; Klompmaker, R.; Freire, R.; Clouin, C.; Taylor, S. S.; Yaffe, M. B.; Medema, R. H. Polo-like kinase-1 is activated by aurora A to promote checkpoint recovery. *Nature* **2008**, *455*, 119−123.
(33) Seki, A.; Coppinger, J. A.; Jang, C.-Y.; Yates, J. R.; Fang, G. Bora and the Kinase Aurora A Cooperatively Activate the Kinase Plk1 and Control Mitotic Entry. *Science* **2008**, *320*, 1655−1658.
(34) Feine, O.; Hukasova, E.; Bruinsma, W.; Freire, R.; Fainsod, A.; Gannon, J.; Mahbubani, H. M.; Lindqvist, A.; Brandeis, M. Phosphorylation-mediated stabilization of Bora in mitosis coordinates Plx1/Plk1 and Cdk1 oscillations. *Cell Cycle* **2014**, *13*, 1727−1736.
(35) Lee, Y.-C.; Liao, P.-C.; Liou, Y.-C.; Hsiao, M.; Huang, C.-Y.; Lu, P.-J. Glycogen synthase kinase 3 β activity is required for hBora/Aurora A-mediated mitotic entry. *Cell Cycle* **2013**, *12*, 953−960.
(36) Tavernier, N.; Noatynska, A.; Panbianco, C.; Martino, L.; van Hove, L.; Schwager, F.; Léger, T.; Gotta, M.; Pintard, L. Cdk1 phosphorylates SPAT-1/Bora to trigger PLK-1 activation and drive mitotic entry in C. elegans embryos. *J. Cell Biol.* **2015**, *208*, 661−669.
(37) Hutterer, A.; Berdnik, D.; Wirtz-Peitz, F.; Žigman, M.; Schleiffer, A.; Knoblich, J. A. Mitotic Activation of the Kinase Aurora-A Requires Its Binding Partner Bora. *Dev. Cell* **2006**, *11*, 147−157.
(38) Seki, A.; Coppinger, J. A.; Du, H.; Jang, C.-Y.; Yates, J. R.; Fang, G. Plk1- and -TrCP-dependent degradation of Bora controls mitotic progression. *J. Cell Biol.* **2008**, *181*, 65−78.
(39) Bayliss, R.; Sardon, T.; Vernos, I.; Conti, E. Structural basis of Aurora-A activation by TPX2 at the mitotic spindle. *Mol. Cell* **2003**, *12*, 851−862.
(40) Lee, C.-R.; Park, Y.-H.; Kim, Y.-R.; Peterkofsky, A.; Seok, Y.-J. Phosphorylation-Dependent Mobility Shift of Proteins on SDS-PAGE is Due to Decreased Binding of SDS. *Bull. Korean Chem. Soc.* **2013**, *34*, 2063−2066.
(41) Lindqvist, A.; Rodríguez-Bravo, V.; Medema, R. H. The decision to enter mitosis: feedback and redundancy in the mitotic entry network. *J. Cell Biol.* **2009**, *185*, 193−202.
(42) Xu, J.; Shen, C.; Wang, T.; Quan, J. Structural basis for the inhibition of Polo-like kinase 1. *Nat. Struct. Mol. Biol.* **2013**, *20*, 1047−1053.
(43) Merkley, E. D.; Rysavy, S.; Kahraman, A.; Hafen, R. P.; Daggett, V.; Adkins, J. N. Distance restraints from crosslinking mass spectrometry: mining a molecular dynamics simulation database to evaluate lysine-lysine distances. *Protein Sci.* **2014**, *23*, 747−759.
(44) Dang, X.; Scotcher, J.; Wu, S.; Chu, R. K.; Tolić, N.; Ntai, I.; Thomas, P. M.; Fellers, R. T.; Early, B. P.; Zheng, Y.; Durbin, K. R.; Leduc, R. D.; Wolff, J. J.; Thompson, C. J.; Pan, J.; Han, J.; Shaw, J. B.; Salisbury, J. P.; Easterling, M.; Borchers, C. H.; Brodbelt, J. S.; Agar, J. N.; Paša-Tolić, L.; Kelleher, N. L.; Young, N. L. The first pilot project of the consortium for top-down proteomics: a status report. *Proteomics* **2014**, *14*, 1130−1140.
(45) Zheng, Y.; Fornelli, L.; Compton, P. D.; Sharma, S.; Canterbury, J.; Mullen, C.; Zabrouskov, V.; Fellers, R. T.; Thomas, P. M.; Licht, J. D.; Senko, M. W.; Kelleher, N. L. Unabridged Analysis of Human Histone H3 by Differential Top-Down Mass Spectrometry Reveals Hypermethylated Proteoforms from MMSET/NSD2 Overexpression. *Mol. Cell. Proteomics* **2016**, *15*, 776−790.

DOI: 10.1021/acscentsci.6b00053
ACS Cent. Sci. 2016, 2, 445−455